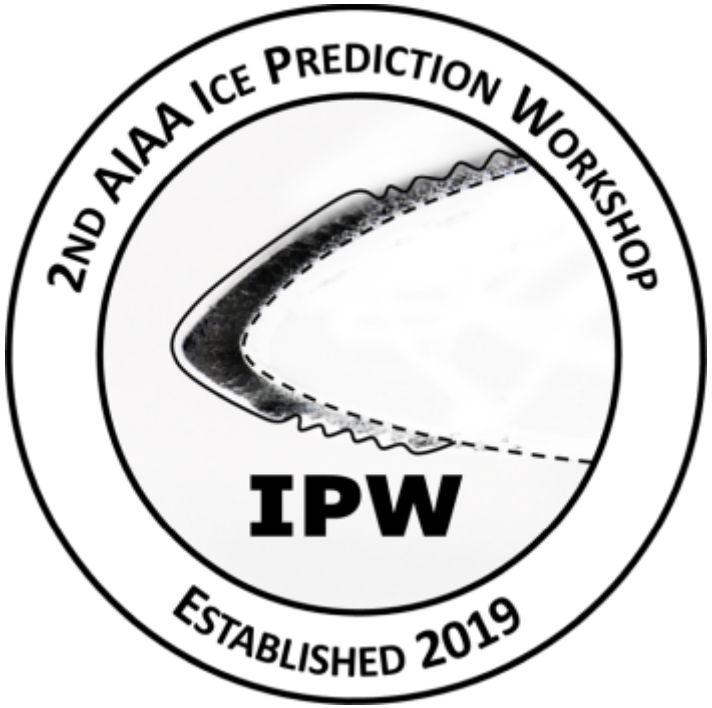

June 23, 2023

JAXA results in IPW2

Kei Shimura and Yuki Ide
Japan Aerospace Exploration Agency (JAXA)

Outline

- Code description
- Case 1 (CRM65 Midspan)
- Case 2 (CRM65 Inboard)
- Case 3 (RG-15)

Code description (1/2): Air and droplet flow analyses

- Air flow solver: JAXA-FaSTAR

  Models

  - Compressible RANS with calorically perfect
  - S-A model with roughness effect (B. Aupoix and P.R. Spalart, 2003.)
  - manually set constant roughness

  Discretization

  - SLAU2 with 2nd-order MUSCL (Advection term), 2nd-order Central difference (Viscous term)
  - LU-SGS (Time integration)

  Shear stress τ_w and heat flux q_w are directly calculated from RANS results.

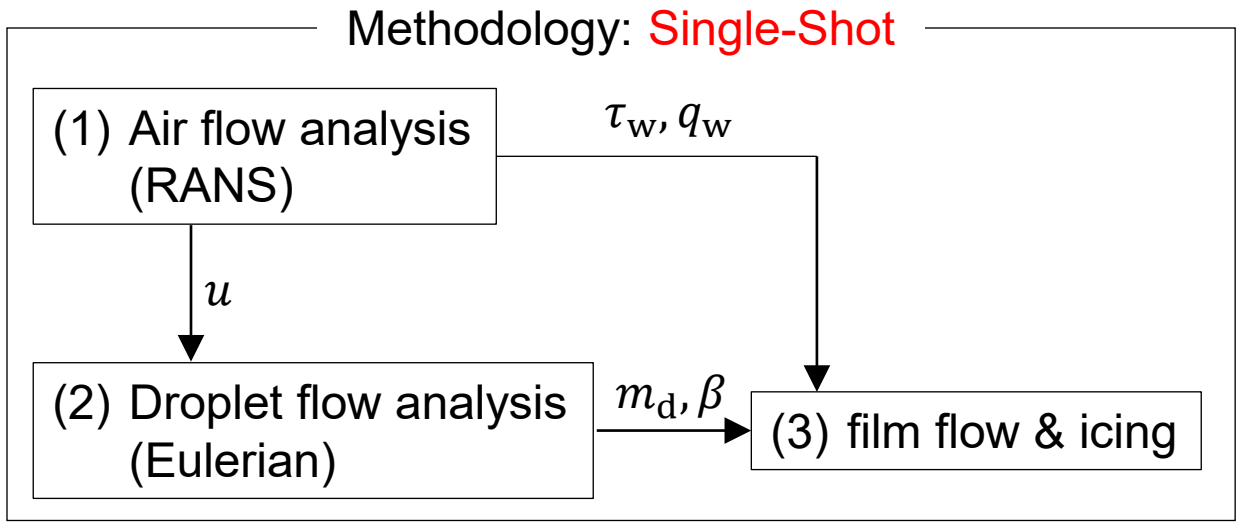

- Droplet flow solver: inviscid eqs in Eulerian framework

  Models

  - Source terms are drag-force for sphere particles (Schiller and Naumann, 1935) and Gravity force

  Discretization

  - 2nd-order upwind scheme (Advection), Euler explicit method (Time integration)

Code description (2/2): Shallow water film flow analysis (icing)

Models

- Shallow-Water Icing Model (SWIM)
- Source terms
  - Droplet impingement
  - Evaporation and sublimation
  - Convective heat transfer
  - Radiation

Discretization

- Finite volume method (Cell-Centered)
- 1st-order upwind scheme (Advection)
- Try and error method (Time integration)

Methodology: Single-Shot

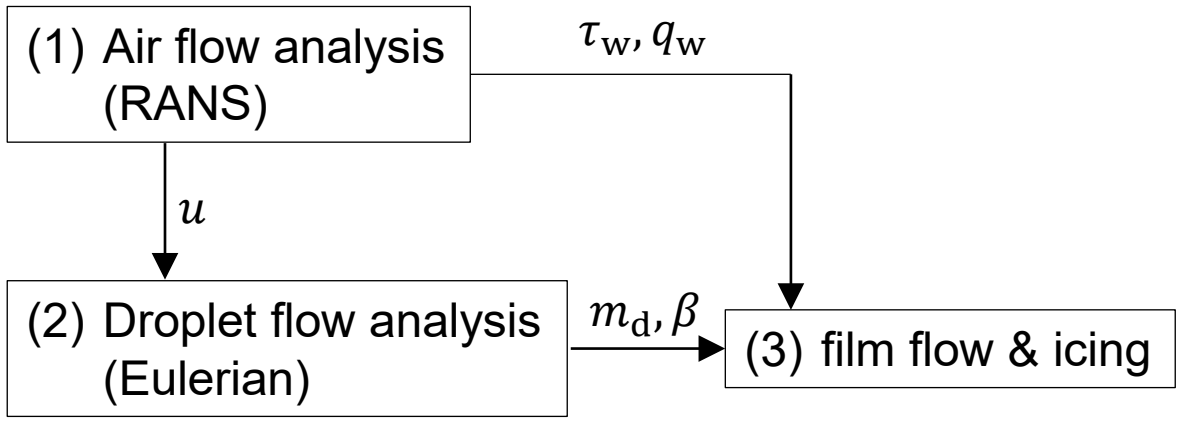

Evaporation at a laminar boundary layer on flat plate

$$\dot{Q}_{es} = -0.5(L_{ev} + L_{su})\frac{0.7}{C_{p,air}}\mathrm{HTC}\left(\frac{p_{v,surf} - \mathrm{Rh}p_{v,e}}{P_e}\right)$$

RANS results-based heat transfer coefficient

$$\mathrm{HTC} = \frac{\kappa_{air}\left.\frac{\partial T_{air}}{\partial y}\right|_{wall}}{T_{rec} - T_{wall}}$$

Summary of simulated cases

- All test cases (9 cases) were simulated.
- Differences due to (given) meshes were evaluated on the basis of air-flow results.
- We submitted data obtained by using “structured mesh with gap”.

Computational time

Case	Mesh	Analysis	MPI threads	Elapsed time [sec]	Number of steps
Case 1.1	Structured with gap	Air flow	144	1212	10000
		Droplet flow	144	1175	20000
		Film & Icing	18	40878	24805000
Case 2.1	Structured with gap	Air flow	144	2117	10000
		Droplet flow	144	1943	20000
		Film & Icing	18	68120	30562000
Case 3.1	Structured	Air flow	9	621	20000
		Droplet flow	9	124	8000
		Film & Icing	2	92	324000

* Flat MPI

* Architecture: FUJITSU PRIMERGY RX2540 M5 (Intel Xeon Gold 6240 × 2 / Node, 36 Core/Node)

Case 1.1 : Air flow, Pressure coefficients

- The predicted Cp distributions show entirely good agreement with those of the experiments, including locations of the attachment line.

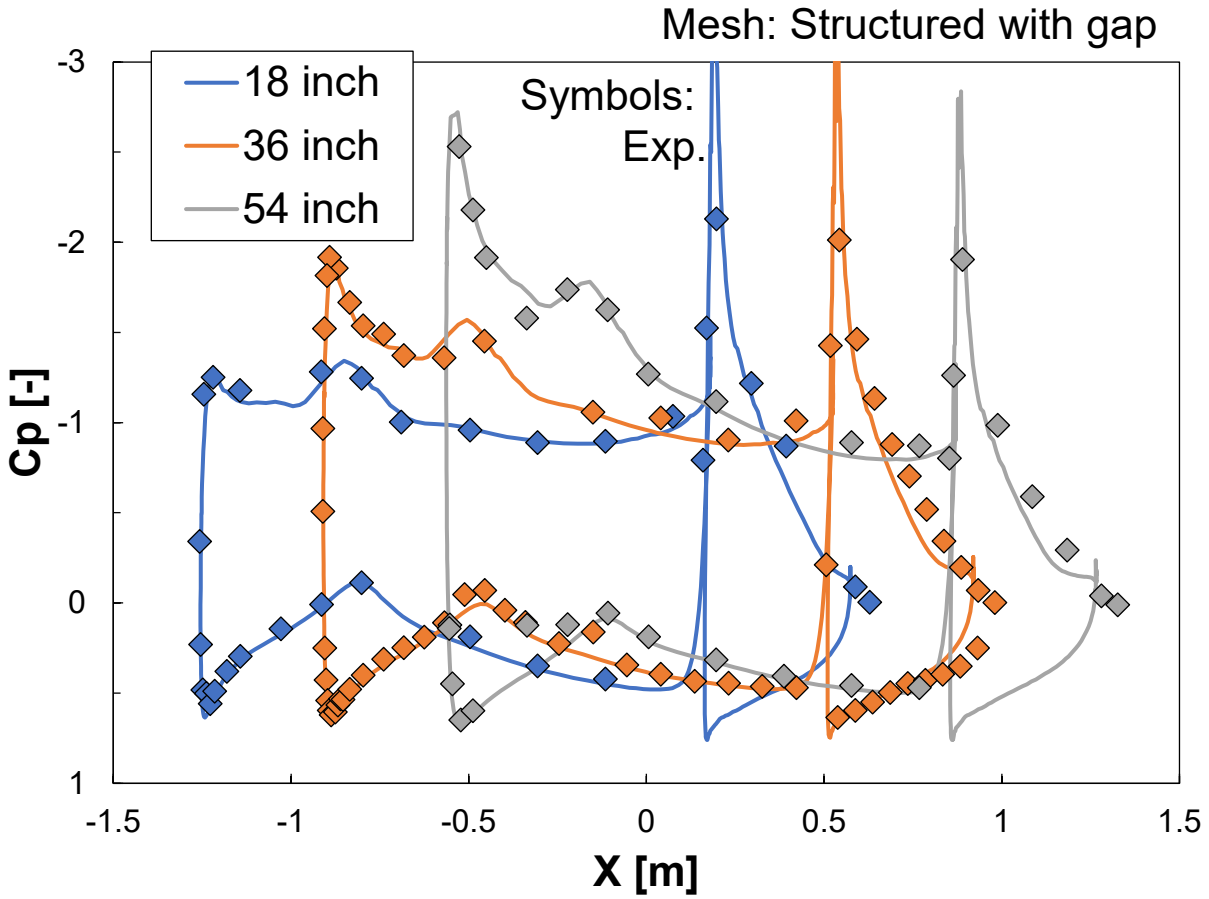

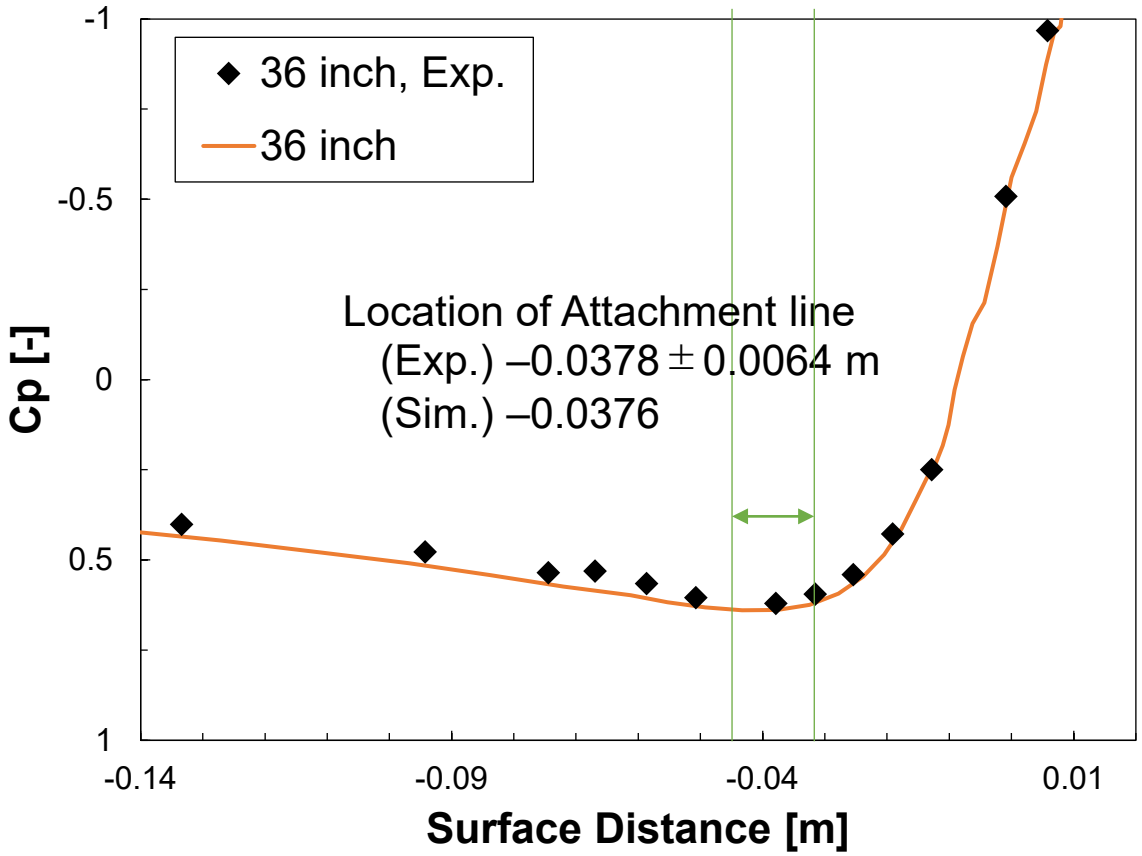

Case 1.1 : Air flow, Differences due to meshes (1/2)

The same trend was obtained as the test case description (predicted by FENSAP-ICE with SA model).

- “Structured mesh without gap” causes large flow separation near the upper channel wall
- Differences at a lower surface, where many droplets impinge, are relatively small so that the influence of neglecting gap may be small for ice accretion simulation.

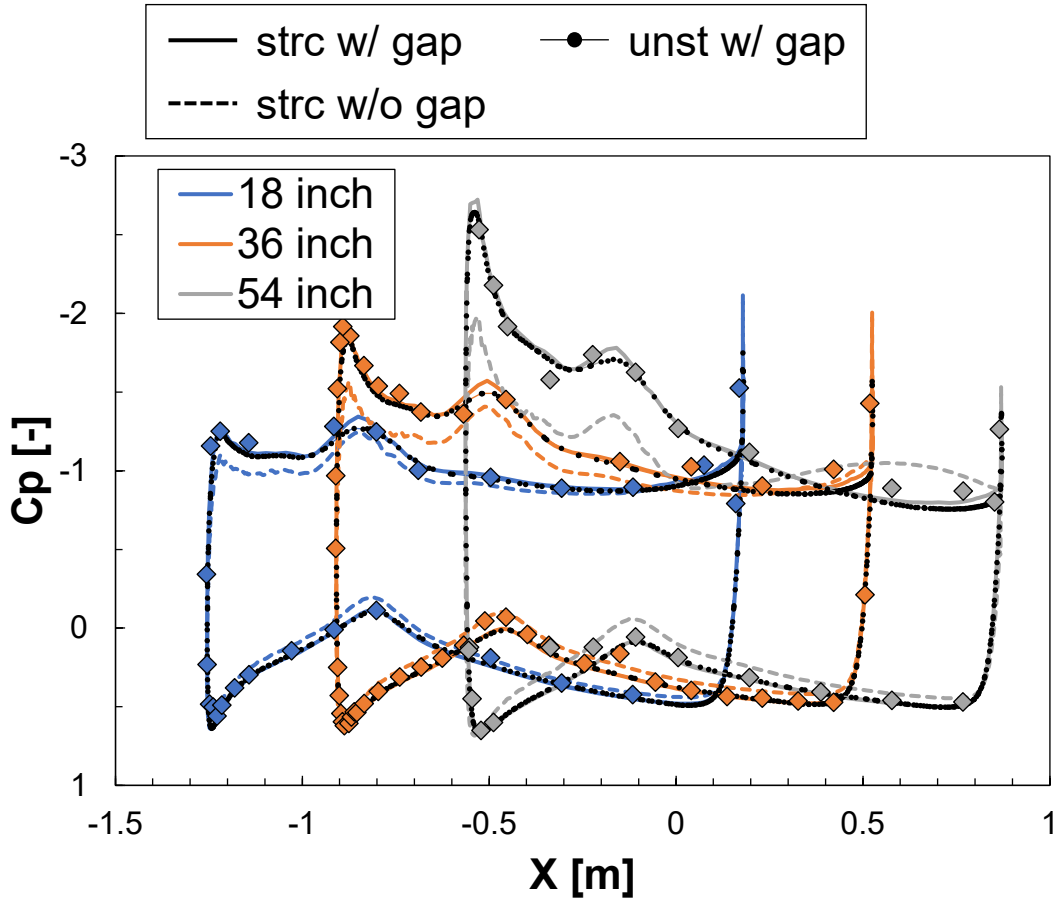

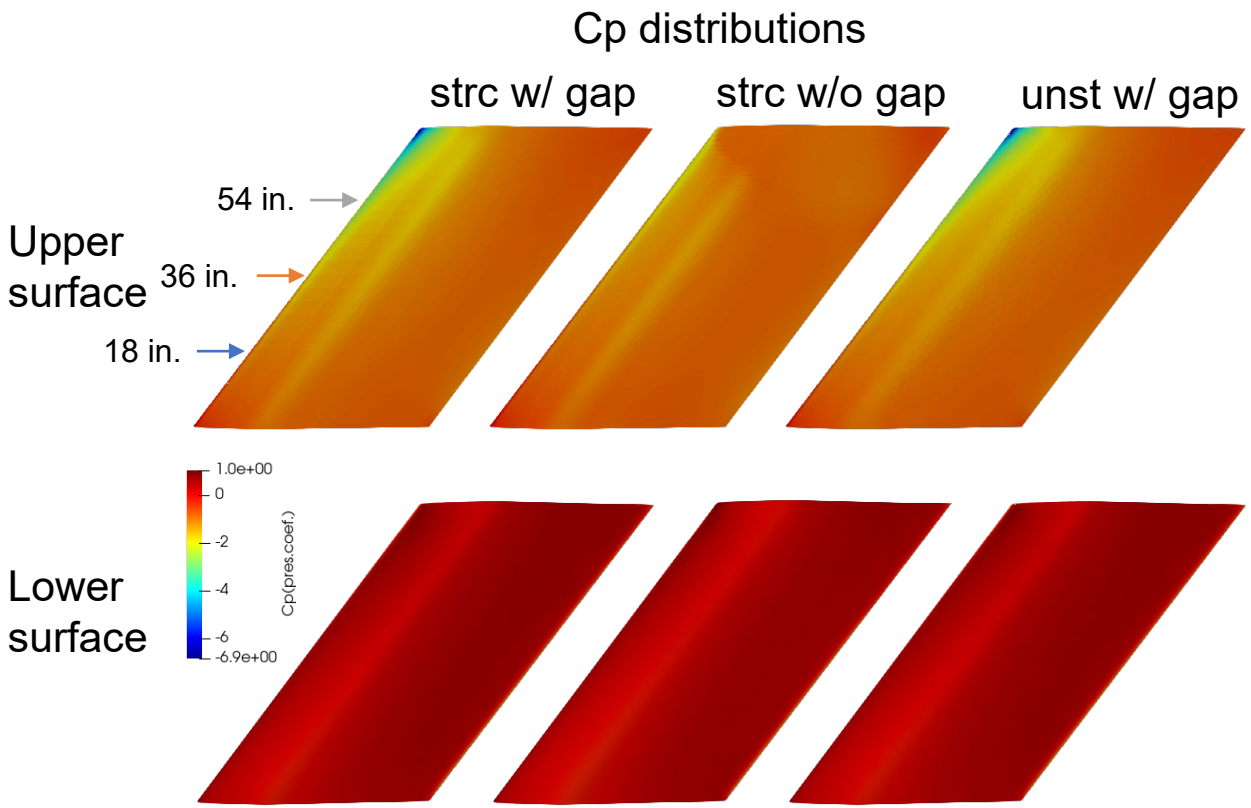

Case 1.1 : Air flow, Differences due to meshes (2/2)

The structured mesh shows the oscillation in shear stress, probably due to insufficient resolution of meshes, particularly near the leading-edge.

“Unstructured mesh with gap” shows the best results in terms of Cp and Cf.

- But, this mesh had poor convergence for air and film flow analyses.
- Thus, “Structured mesh with gap” is selected for further studies.

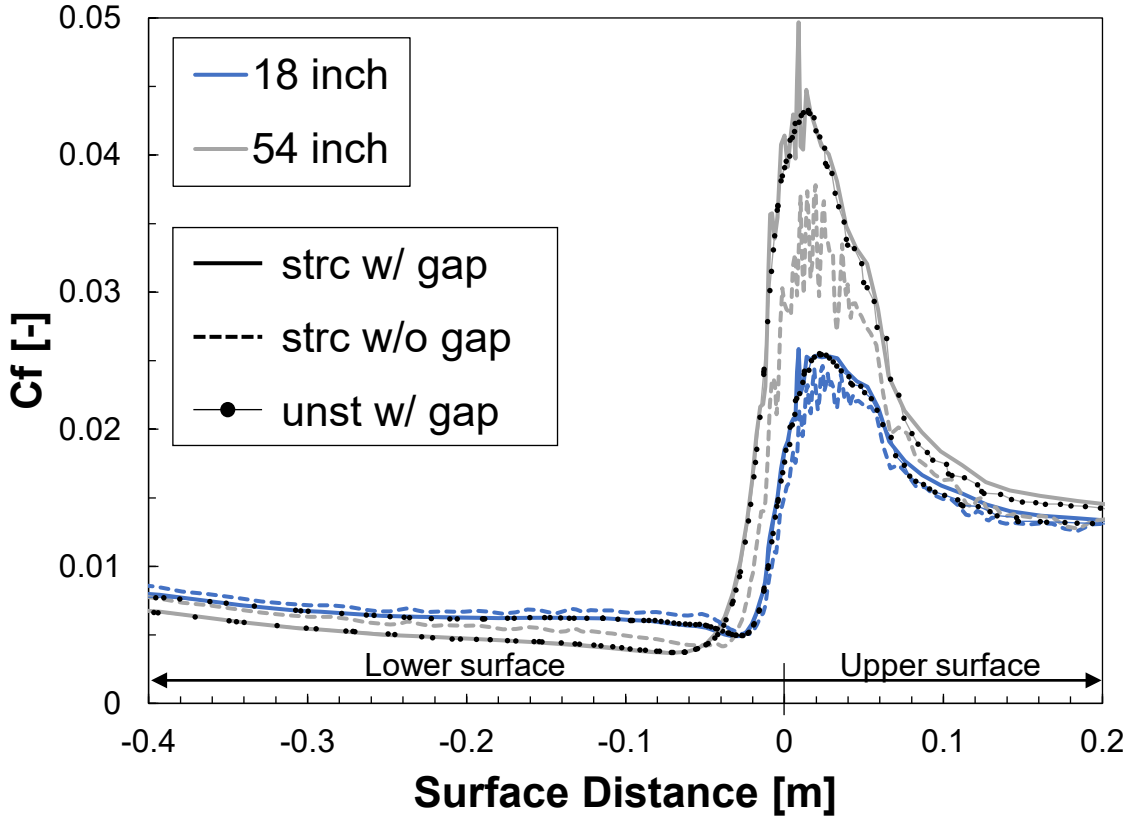

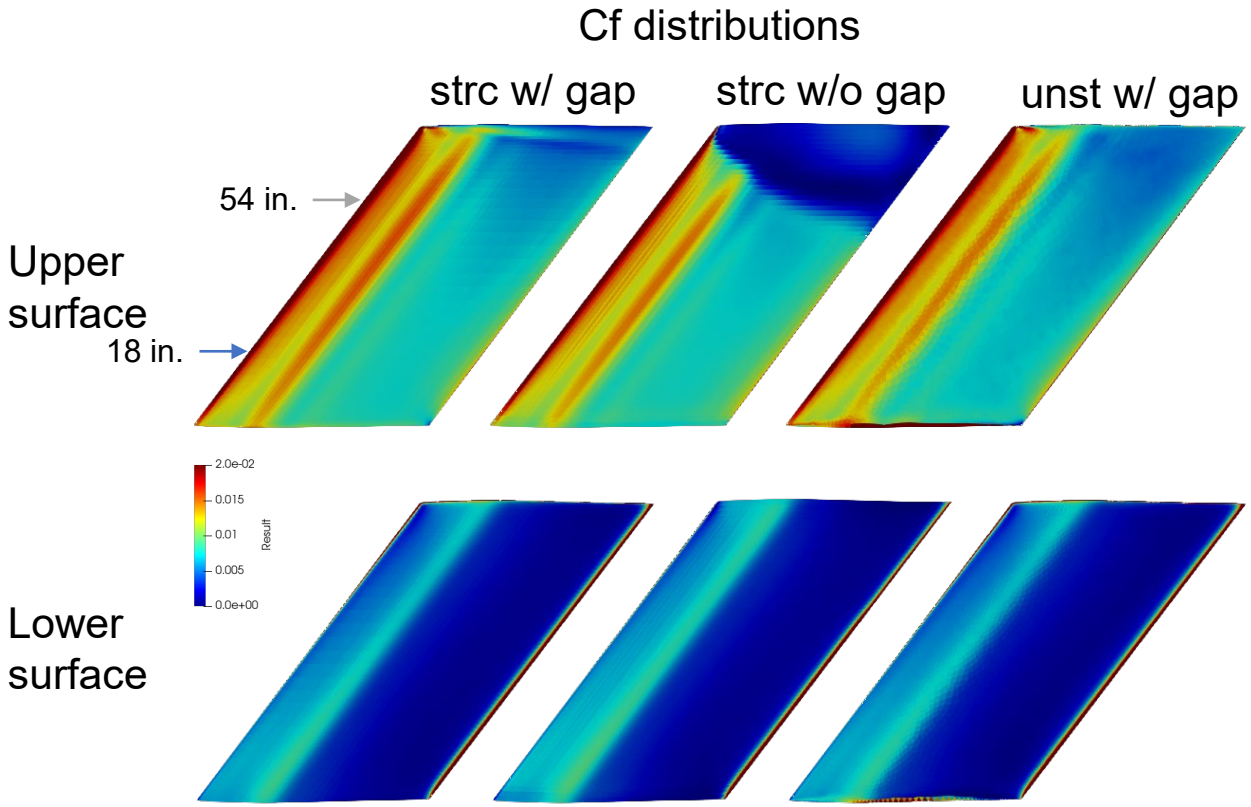

Case 1 : HTC and β

- Collection efficiencies in all 3 cases coincide and are in line with those in other CFD results in WS.
- As with Cf, HTC also shows oscillation near the attachment line on upper surface.

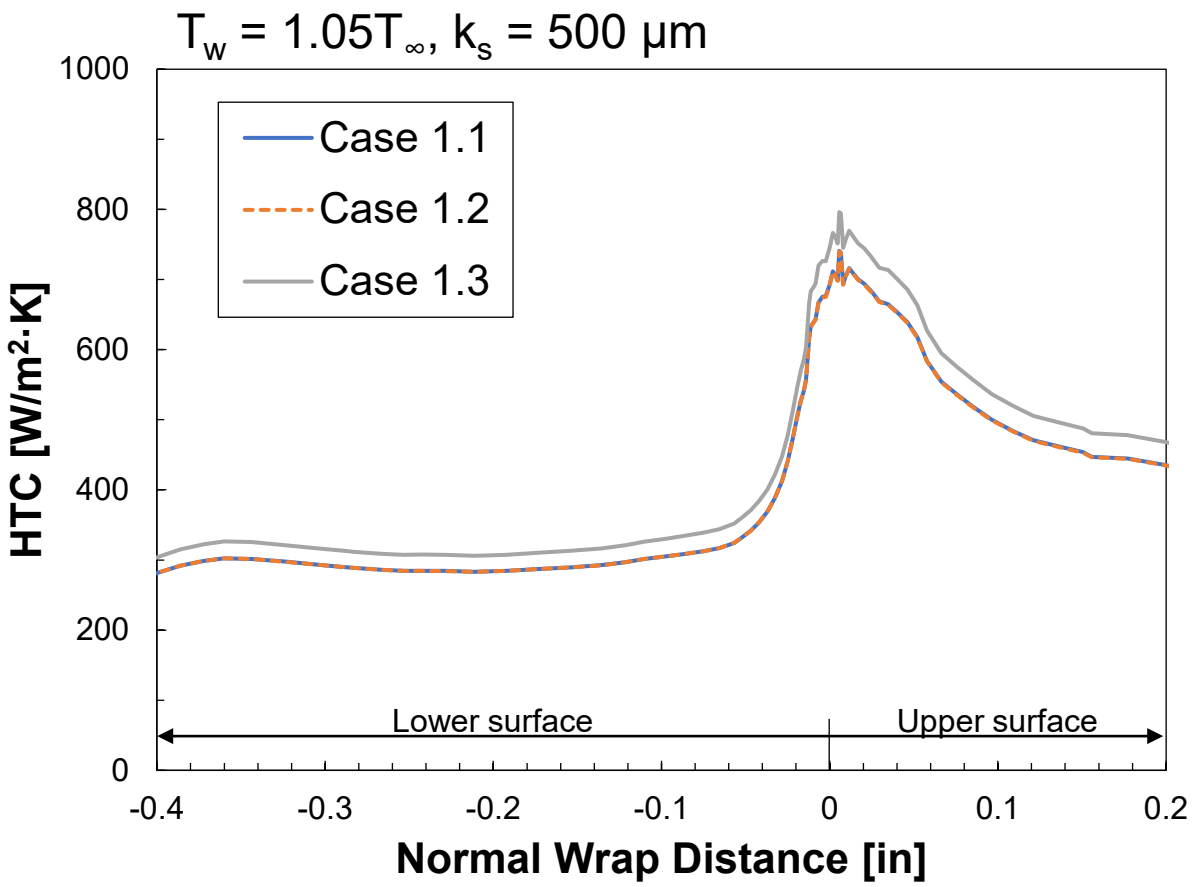

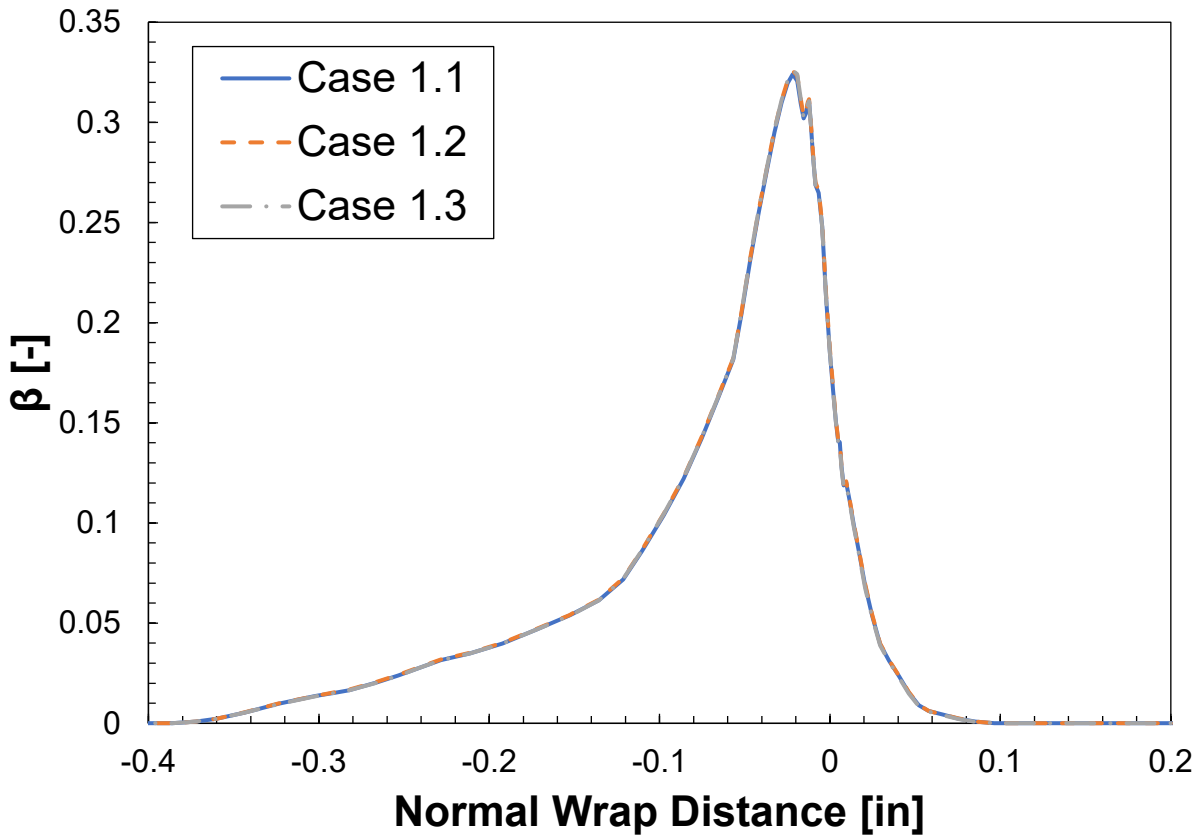

Case 1 : MCCS

- In Cases 1.1 and 1.3, types of ices, namely glaze or rime, are successfully captured.
- In Case 1.2, showing mixed characteristics of glaze and rime, our solver predicts fully rimed ice.

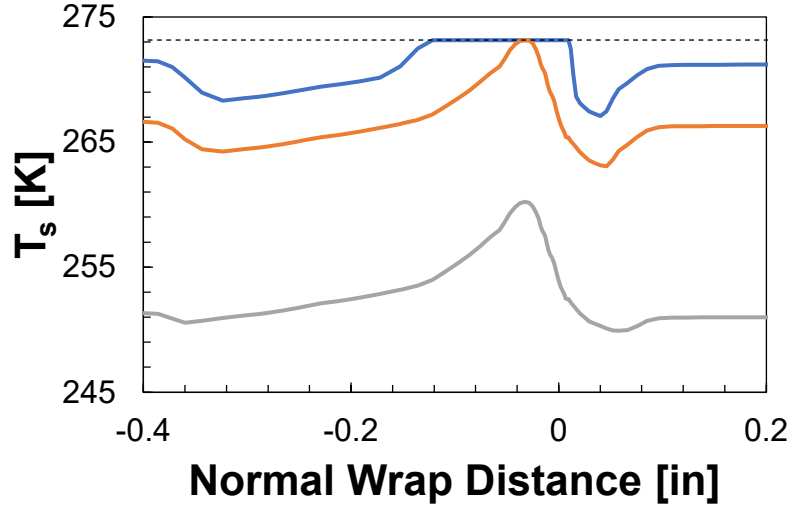

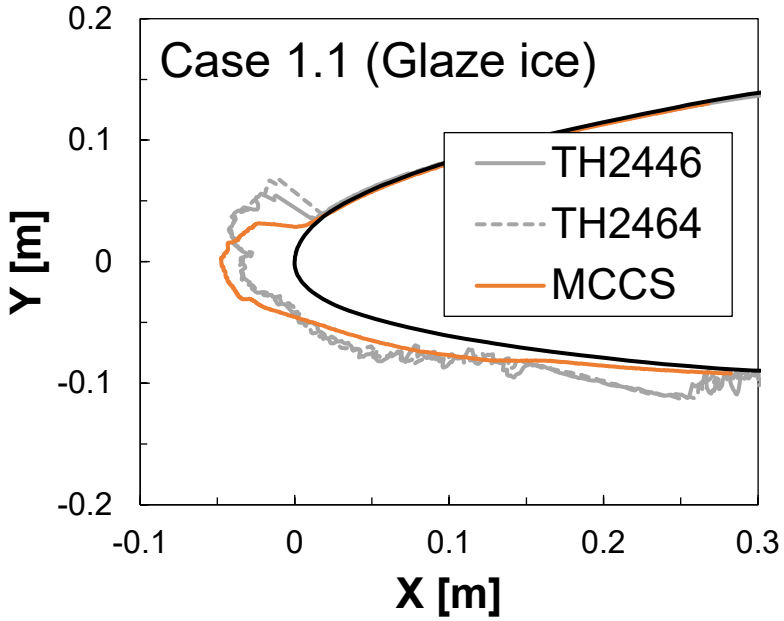

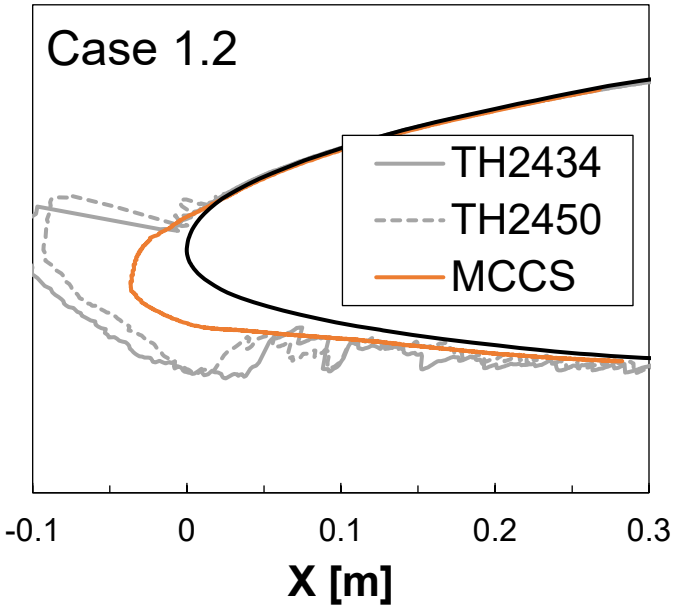

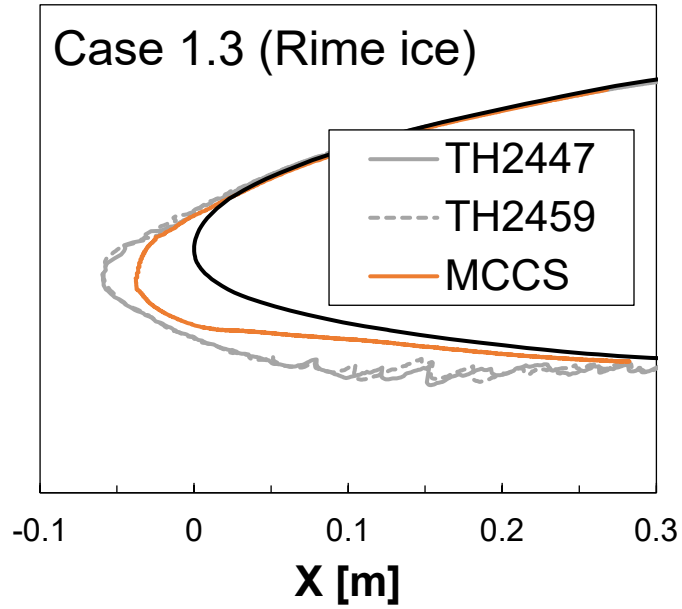

Case 2.1 : Air flow, Pressure coefficients

- Cp distributions including locations of attachment line show good agreement with the experiments.
- Small oscillations are observed on upper surface, but again this may be small influence for icing accretion.

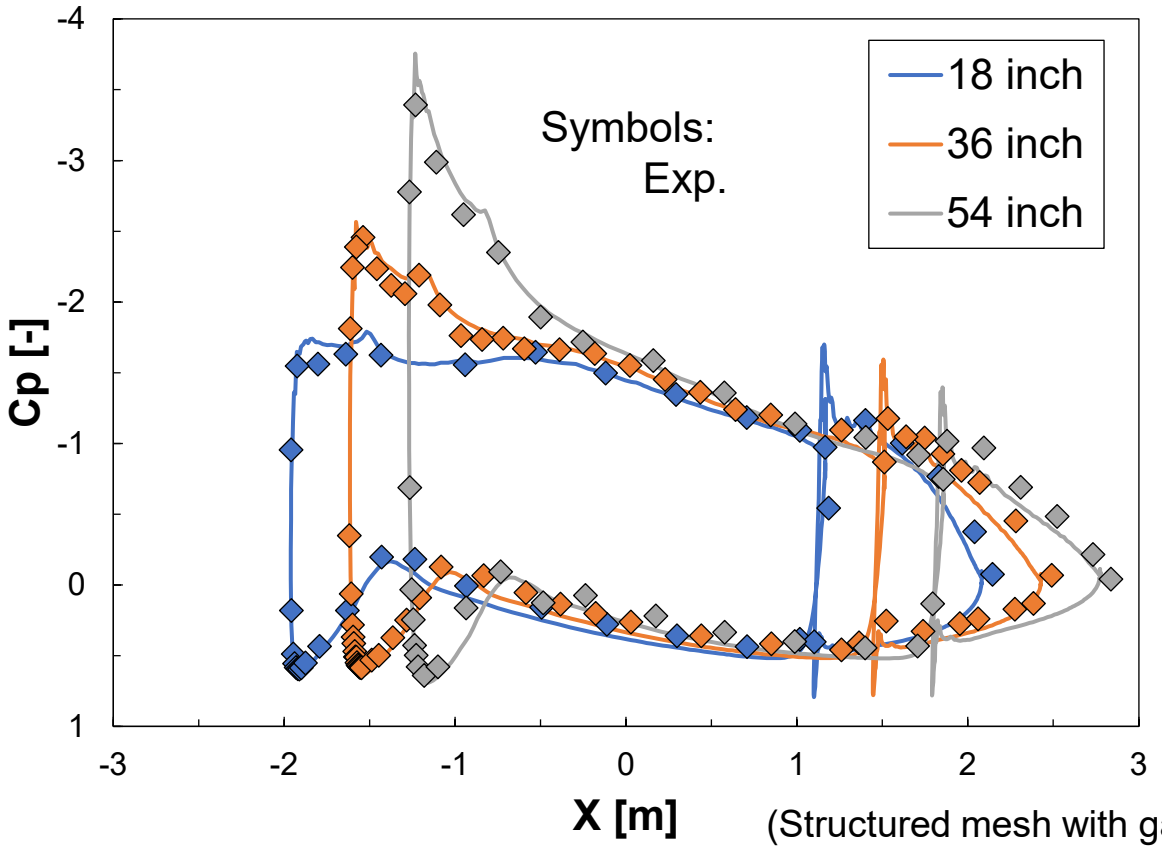

(Structured mesh with gap only)

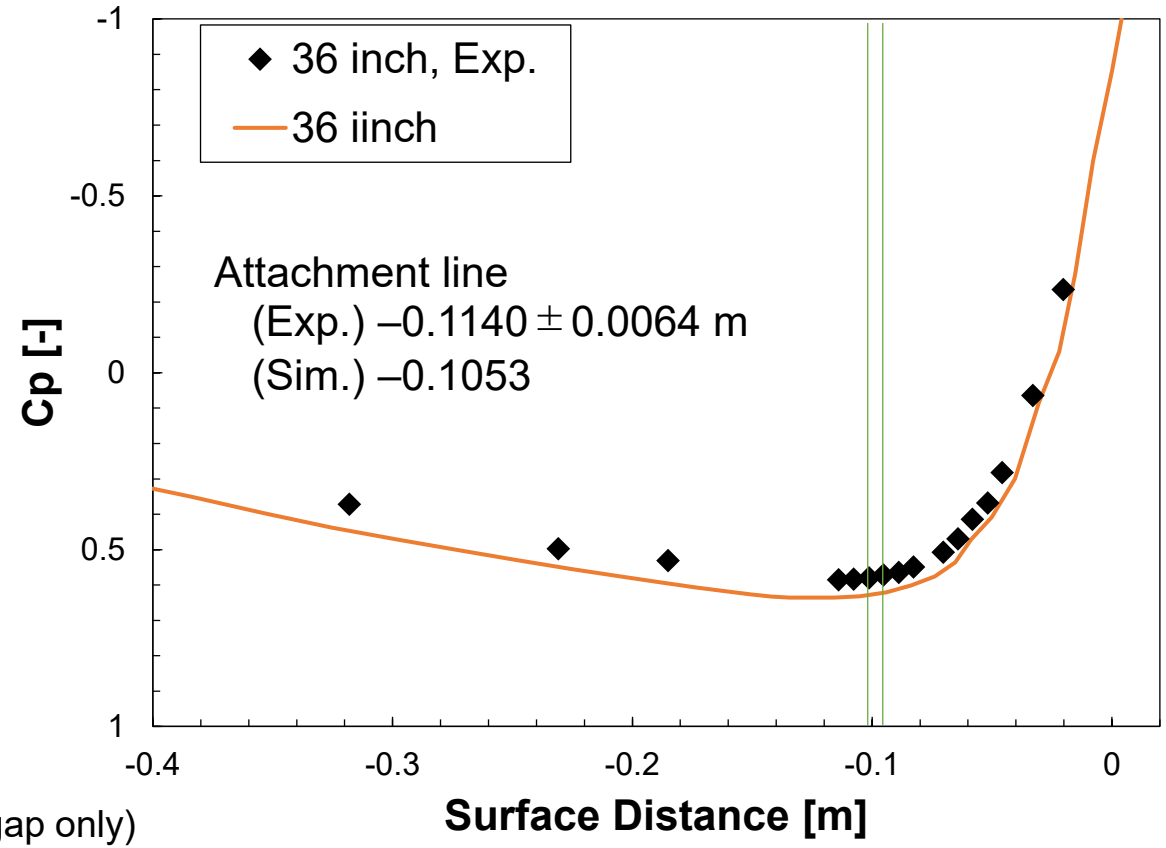

Case 2.1 : Air flow, Differences due to meshes

The same trend was obtained as the test case description and those in Case 1.

- “Structured mesh without gap” causes lower pressure on upper surface due to large flow separation.
- Low resolution meshes cause oscillation of shear stress.
- Although “Unstructured mesh with gap” shows the best results, “Structured mesh with gap” is used for further studies because of poor convergency that unstructured mesh has.

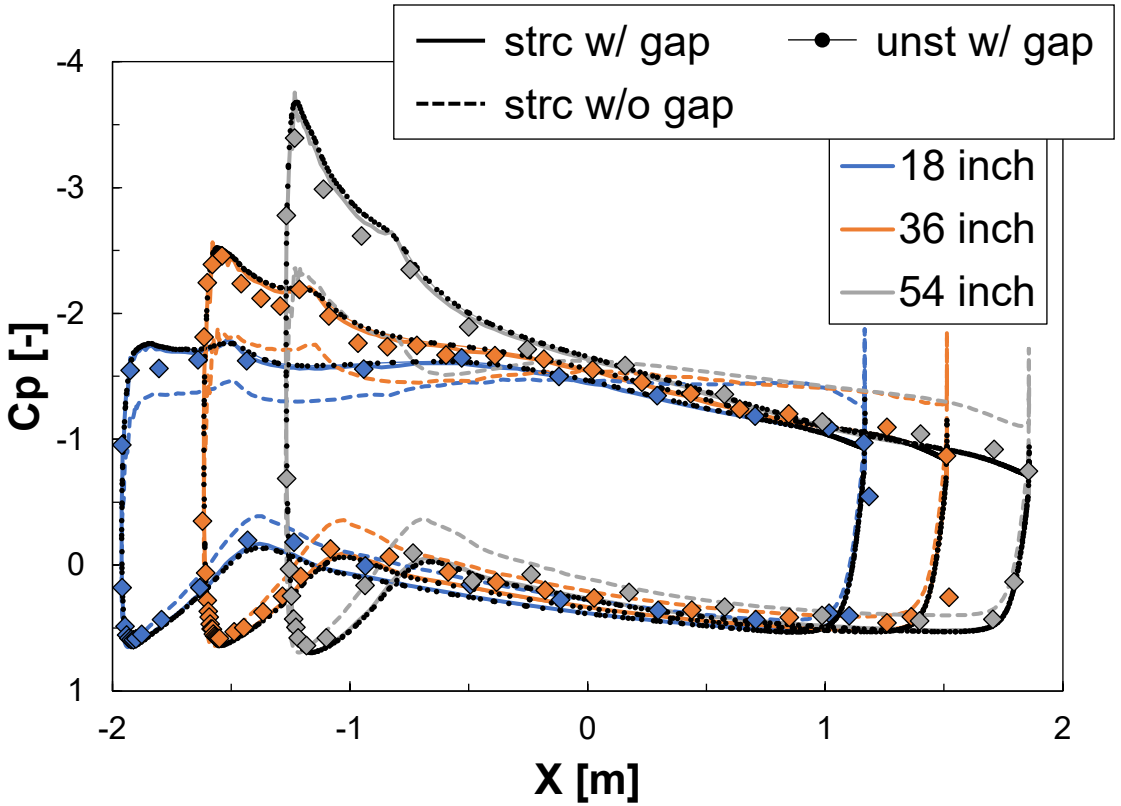

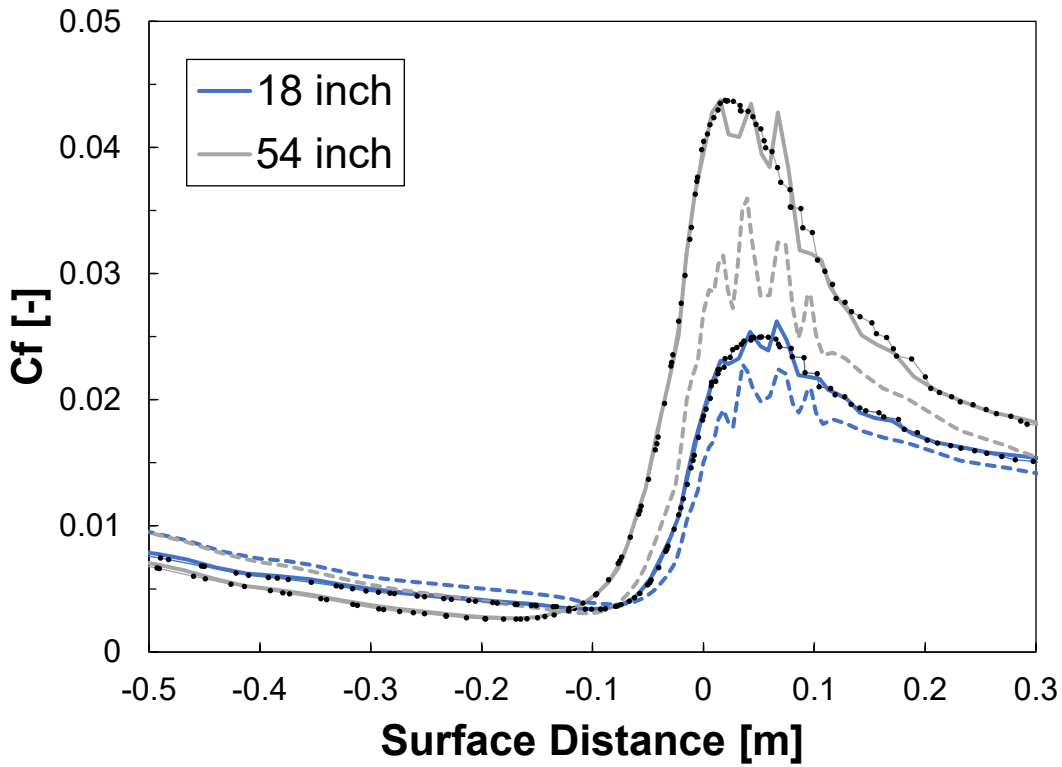

Case 2 : HTC and β

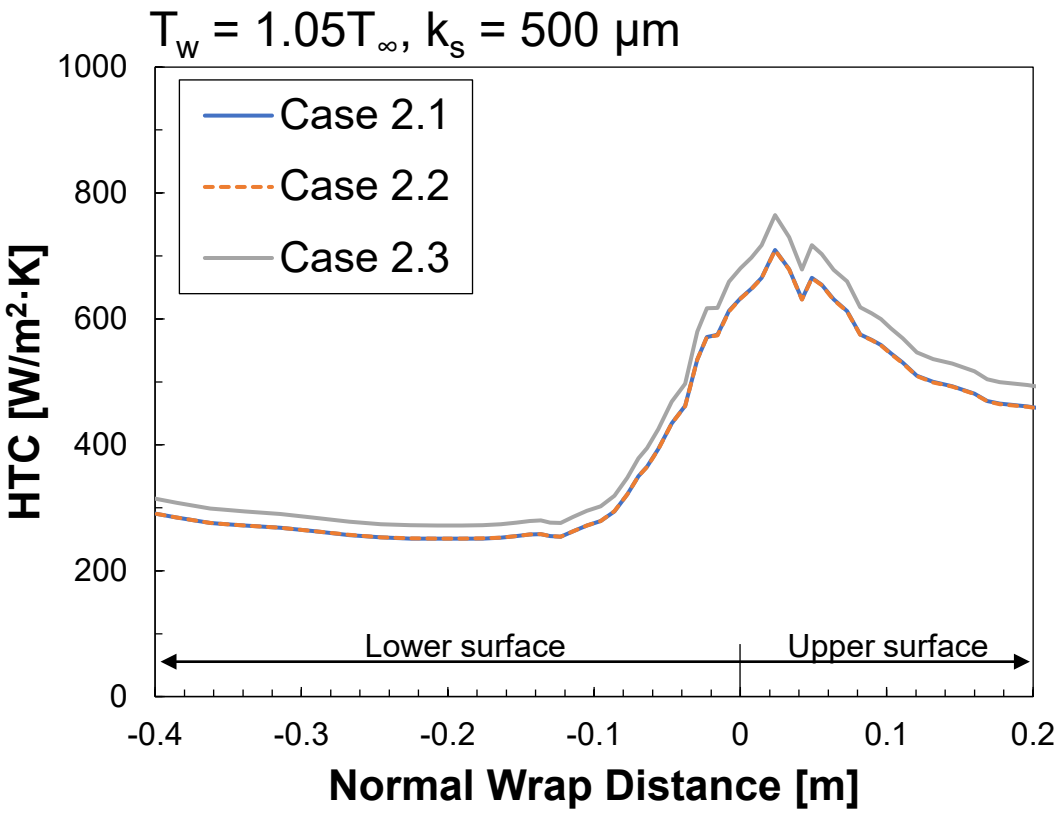

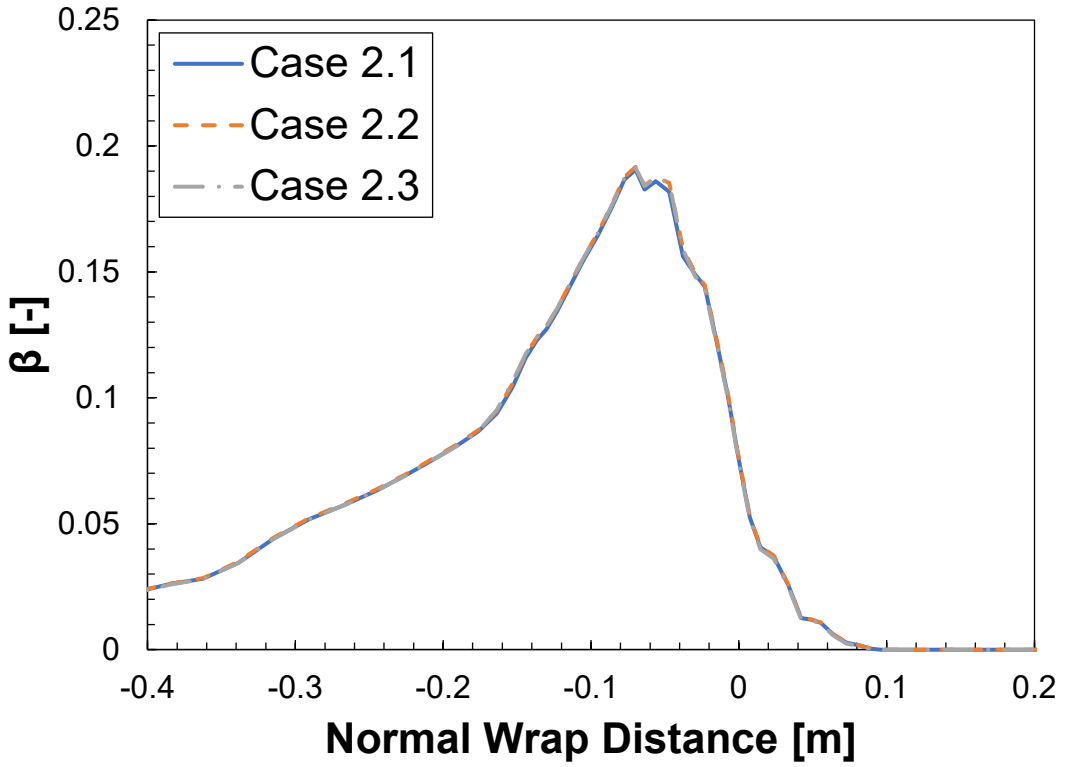

Case 2 : MCCS

Similar trends as Case 1 were observed.

- In Cases 2.1 and 2.3, types of ices, namely glaze or rime, are successfully captured.
- In Case 2.2, showing mixed characteristics of glaze and rime, our solver predicts fully rimed ice.

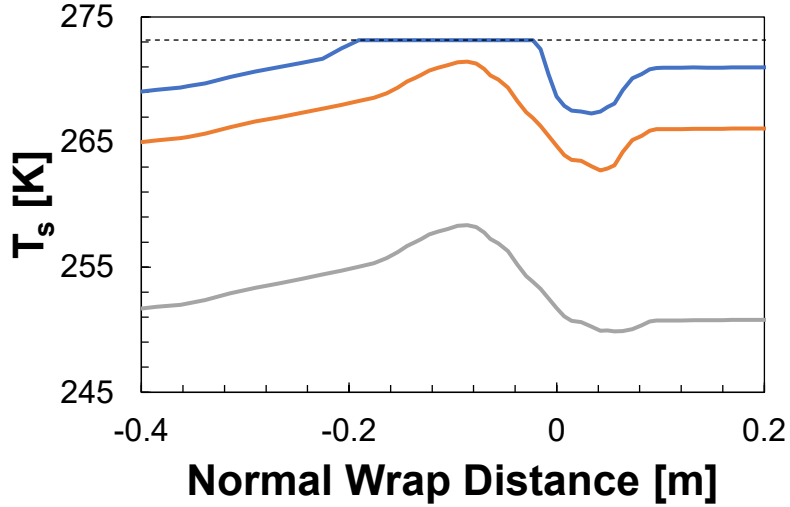

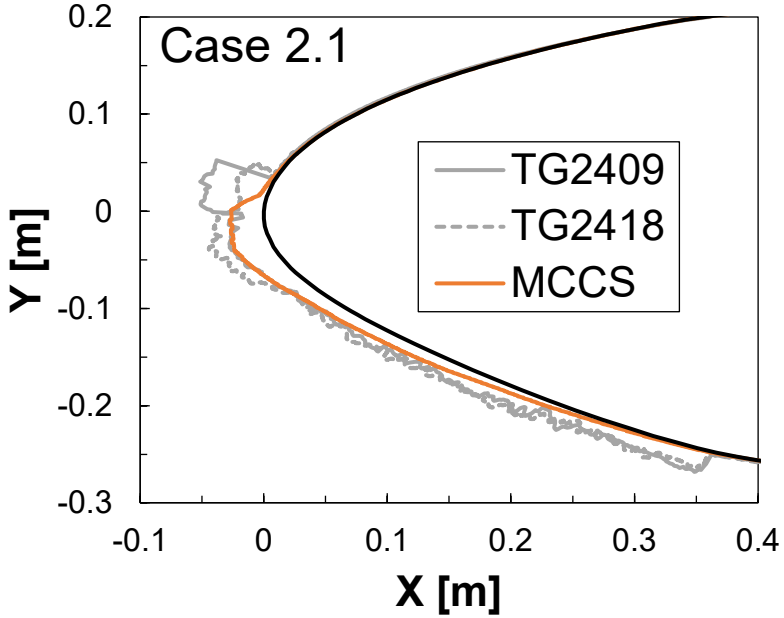

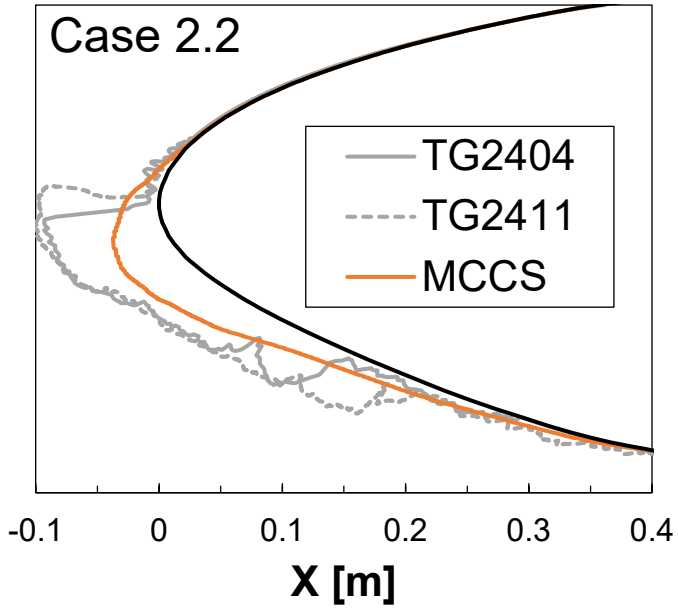

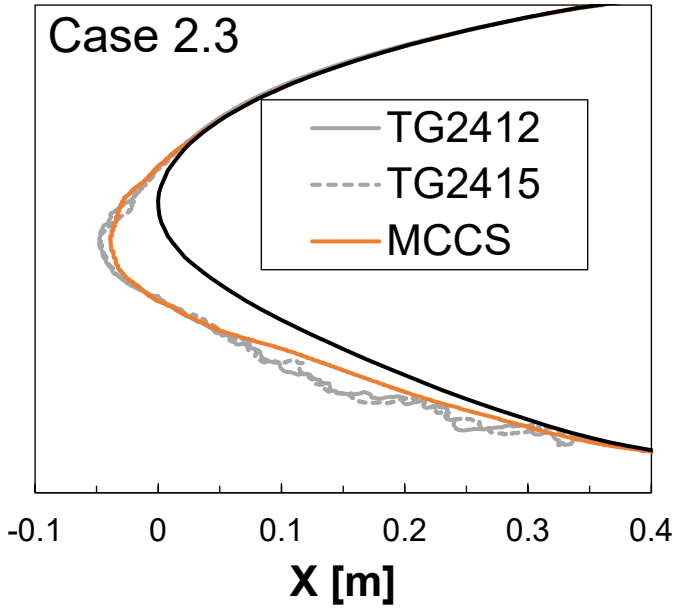

Case 3 : MCCS

- Only structured mesh was tested (effects of meshes are not investigated).
- Similar trends as Cases 1 and 2 in terms of types of ices

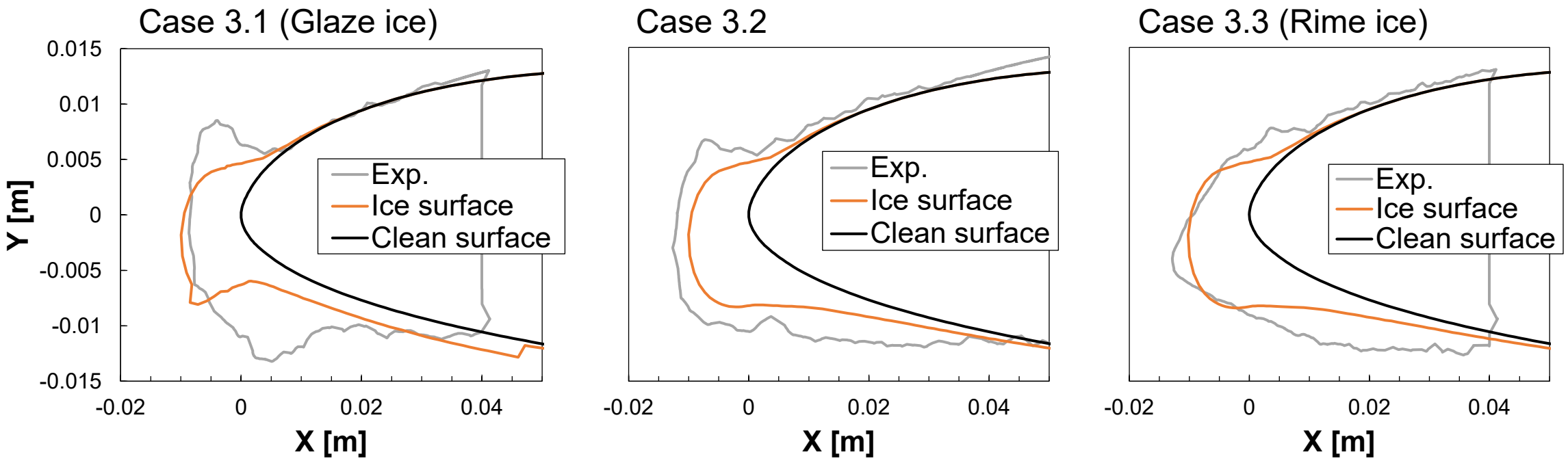

Effects of laminar-turbulent transition (IPW1;NACA23012)

- Effects of transition model
  - Turbulence viscosity on attachment line has large effect for predicting HTC distribution.
  - Fully turbulence assumption may be broken near attachment line.

  Use of transition models can improve accuracy because HTC and shear stress are strongly influenced by transition.

  However, there are large differences between transition models.

(Transition models were not used in IPW2 due to calculation instability.)

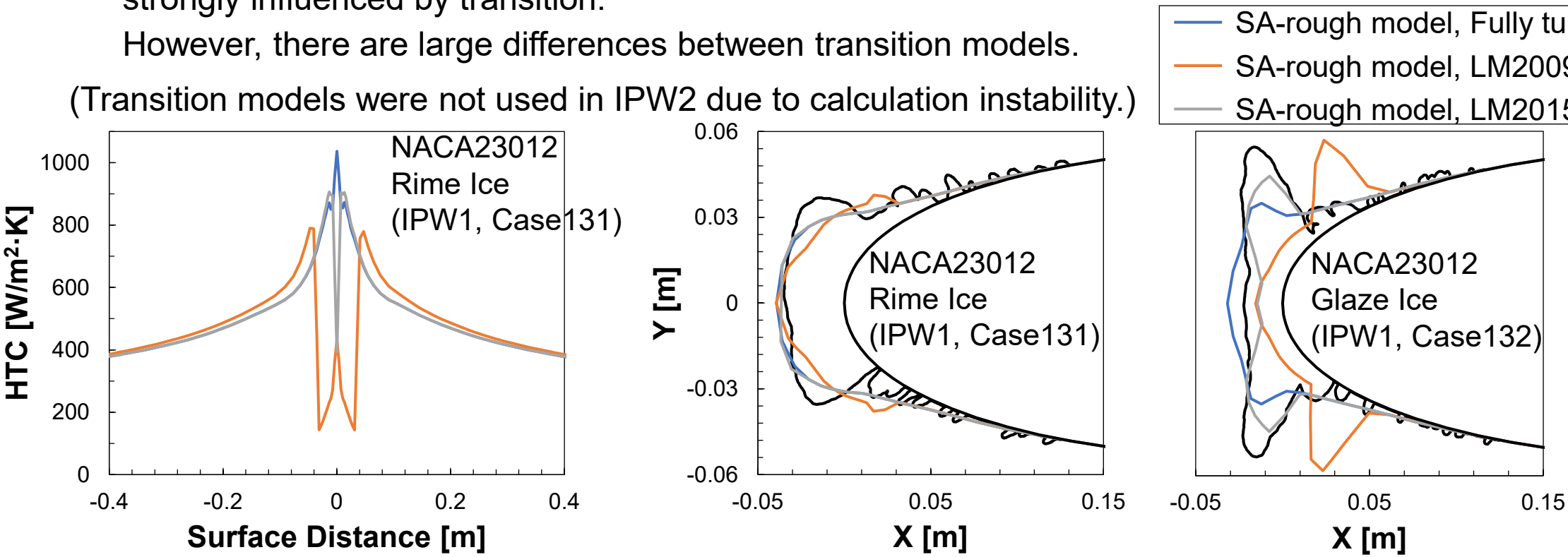

Summary

- Simulation results
  - Single-shot-based simulations were used.
  - In terms of Cp distribution, “Unstructured mesh with gap” gave the best results, but we used “Structured mesh with gap” because of poor convergency in shallow water film flow analysis.
  - Collection efficiencies were in line with those in other CFD results in WS. Film flow & icing analyses could successfully capture types of accreted ice (glaze or rime) in all Cases except Cases X.2, where ices are intermediate shapes of glaze and rime.

Code information: Droplet flow analysis

- Governing equations

  Droplet motion was treated by Eulerian framework.

  Equations are normalized by droplet bulk density of uniform flow, $\rho_{\mathrm{w}}\alpha_{\mathrm{d},\infty}$.

  - Mass conservation

$$\frac{\partial \alpha_{\mathrm{d}}}{\partial t} + \nabla \cdot (\alpha_{\mathrm{d}} \boldsymbol{u}_{\mathrm{d}}) = 0$$

  - Momentum conservation

$$\frac{\partial}{\partial t}(\alpha_{\mathrm{d}} \boldsymbol{u}_{\mathrm{d}}) + \nabla \cdot (\alpha_{\mathrm{d}} \boldsymbol{u}_{\mathrm{d}} \boldsymbol{u}_{\mathrm{d}}) = \boldsymbol{F}_{\mathrm{drag}} + \boldsymbol{F}_{\mathrm{gravity}}$$

  - Drag force

$$\boldsymbol{F}_{\mathrm{drag}} = \frac{3}{4}\frac{\alpha C_{\mathrm{D}}}{\rho_{\mathrm{w}} d^2}\mathrm{Re}_{\mathrm{d}}\mu_{\mathrm{g}}\left(\boldsymbol{u}_{\mathrm{g}} - \boldsymbol{u}_{\mathrm{d}}\right), \qquad \mathrm{Re}_{\mathrm{d}} = \frac{\rho_{\mathrm{g}} d}{\mu_{\mathrm{g}}}\left|\boldsymbol{u}_{\mathrm{g}} - \boldsymbol{u}_{\mathrm{d}}\right|$$

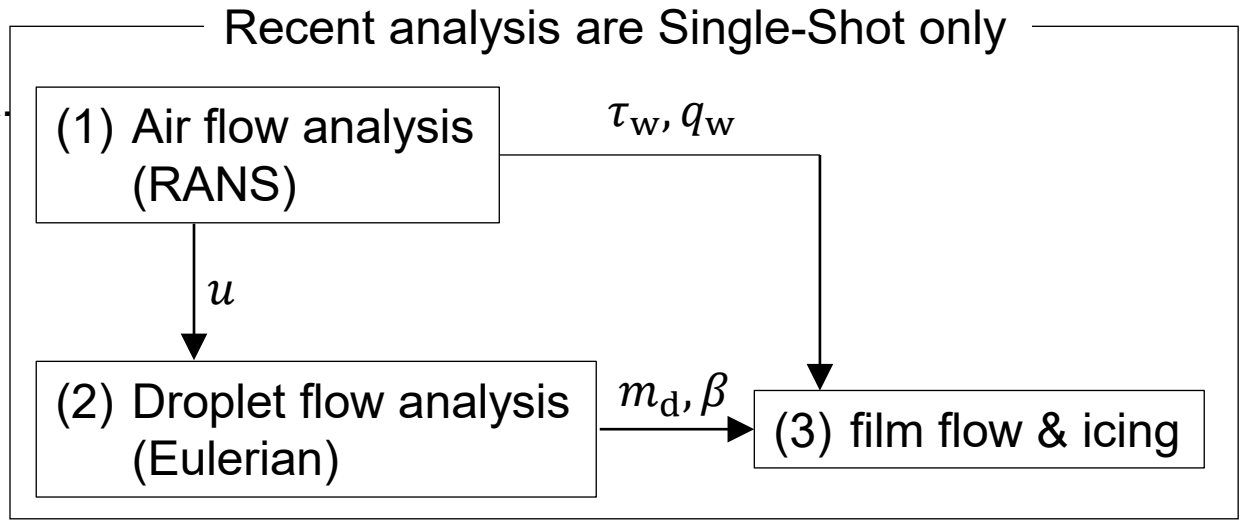

$$C_{\mathrm{D}} = \begin{cases} \frac{24}{\mathrm{Re}_{\mathrm{d}}}\left(1 + 0.15\mathrm{Re}_{\mathrm{d}}^{0.687}\right) & \mathrm{Re}_{\mathrm{d}} \le 1000 \\ 0.4 & \mathrm{Re}_{\mathrm{d}} > 1000 \end{cases}$$

- Discretization : Finite volume method (Cell-Centered)
  - 2nd-order upwind scheme (Advection), Euler explicit method (Time integration)

Code information: Film flow & icing (1/2)

Independent variables : $h_w,\ h_i,\ \bar{T}$

Constants : $\rho_w,\ \rho_i,\ C_{p,w},\ C_{p,i},\ \mu_w,\ L_{fus}$

- Governing equations
  - Mass conservation

$$\rho_w\left[\frac{\partial h_w}{\partial t}+\nabla\cdot(\bar{u}h_w)\right]+\rho_i\frac{\partial h_i}{\partial t}=\dot{m}_{imp}+\dot{m}_{es},\qquad \bar{u}=\frac{h_w}{2\mu_w}\tau_{wall}$$

  - Energy conservation

$$\rho_w C_{p,w}\left[\frac{\partial}{\partial t}(h_w\bar{T})+\nabla\cdot(\bar{u}h_w\bar{T})\right]+\rho_i\frac{\partial}{\partial t}\left[h_i\left(L_{fus}-C_{p,i}\bar{T}\right)\right]=\dot{Q}_{imp}+\dot{Q}_{es}+\dot{Q}_{rad}+\dot{Q}_{conv}$$

  - Compatibility relation

$$h_w\geq 0,\qquad \frac{\partial h_i}{\partial t}\geq 0,\qquad h_w\bar{T}\geq 0,\qquad h_i\bar{T}\leq 0$$

- Constitutive laws

$$\dot{Q}_{es}=-0.5(L_{ev}+L_{su})\frac{0.7}{C_{p,air}}\mathrm{HTC}\left(\frac{p_{v,surf}-\mathrm{Rh}p_{v,e}}{P_e}\right),$$

$$\dot{Q}_{conv}=-\mathrm{HTC}[(\bar{T}+273.15)-T_{rec}]$$

$$\mathrm{HTC}=\frac{\kappa_{air}\left.\frac{\partial T_{air}}{\partial y}\right|_{wall}}{T_{rec}-T_{wall}}$$

Directly calculated from RANS results

Case 3.1 (RG-15), Air and droplet flow analysis

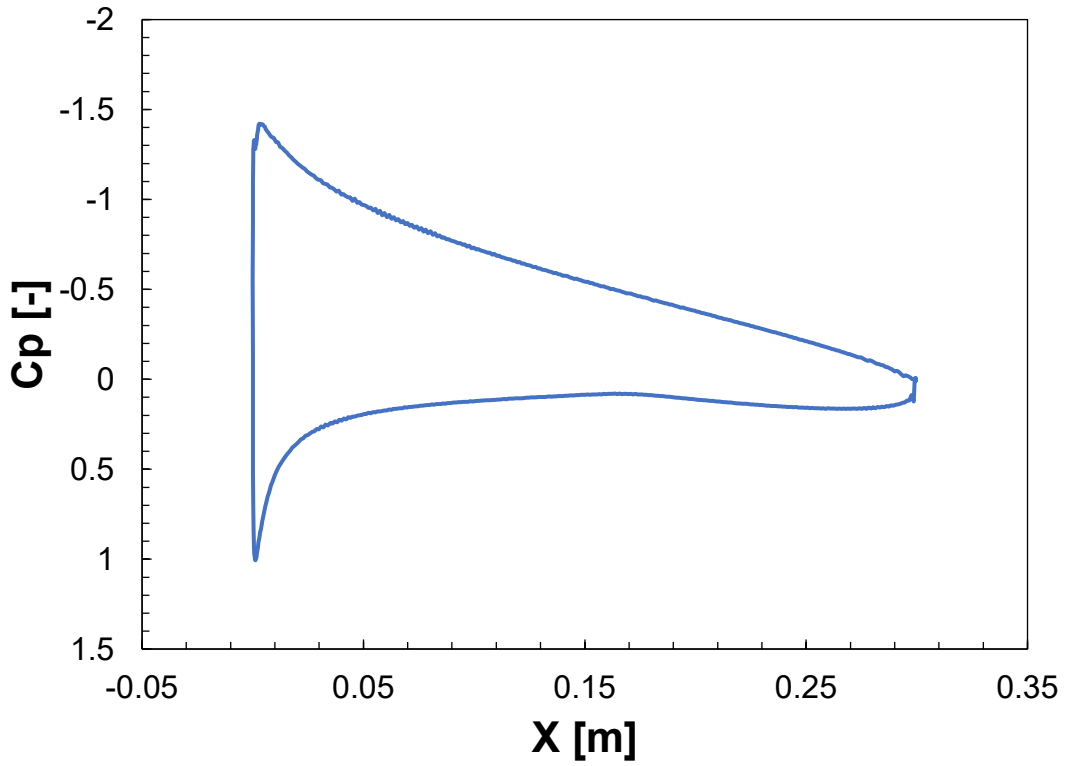

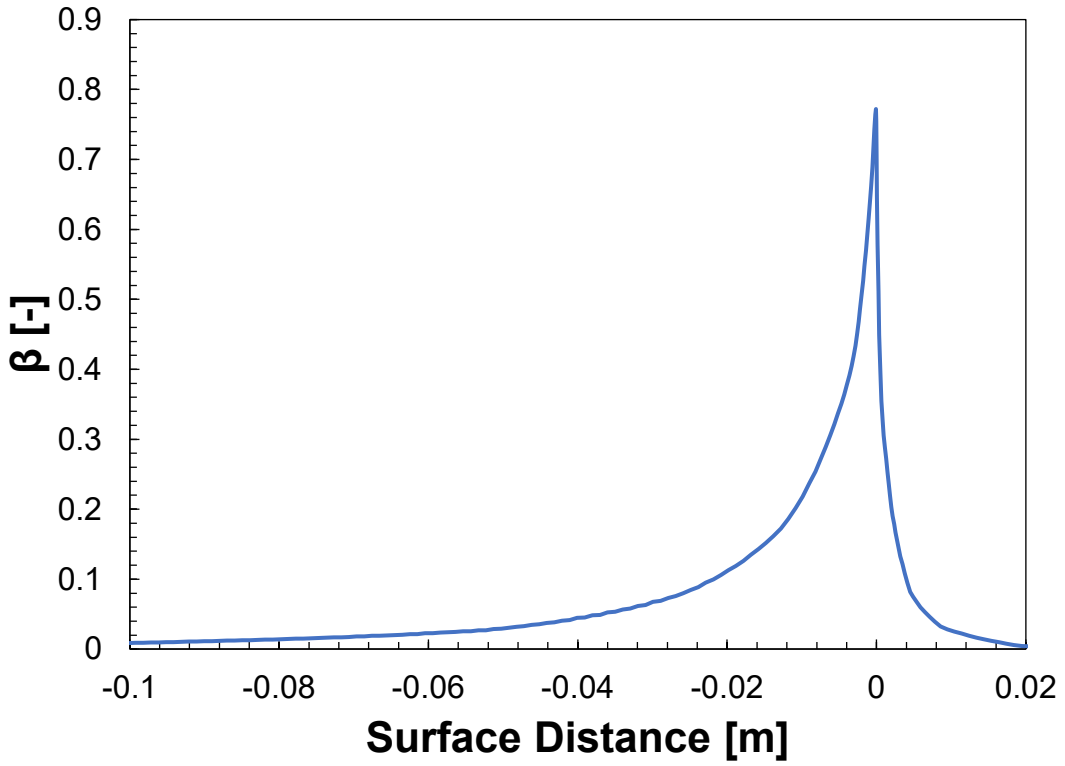

Case 3 (RG-15), film flow & icing, HTC, Ts